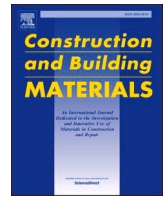




Contents lists available at ScienceDirect

Construction and Building Materials

journal homepage: www.elsevier.com/locate/conbuildmat

Bond performance of fly ash-based geopolymer mortar in simulated concrete sewer substrate

Piumika W. Ariyadasa^a, Allan C. Manalo^{a,*}, Weena Lokuge^a, Vasantha Aravinthan^b, Kiru Pasupathy^a, Andreas Gerdes^c

^a School of Engineering, Centre for Future Materials, University of Southern Queensland, Toowoomba, Queensland 4350, Australia

^b School of Engineering, University of Southern Queensland, Toowoomba, Queensland 4350, Australia

^c Institute for Functional Surfaces, Karlsruhe Institute of Technology, Karlsruhe, Germany

ARTICLE INFO

Keywords:

Geopolymers
Class F fly ash
Slant shear bond strength
Acid resistance
Full-field strain mapping

ABSTRACT

Geopolymers have been extensively explored as a promising repair material for deteriorated Ordinary Portland Cement (OPC) concrete elements. However, knowledge of the adhesion performance of geopolymer to concrete substrates is limited. This study investigates the bond performance of low calcium fly ash geopolymer (FAGP) mortar and concrete for holistic acidic environmental conditions, such as in sewer rehabilitation. The bond evaluation was conducted by slant-shear test, performed at different substrate conditions, namely Rough-Dry, Rough-Saturated, Smooth-Dry and Smooth-Saturated, to simulate the in-service condition of a typical sewer pipe wall. The standard OPC repair mortar and a commercially available proprietary geopolymer repair product (P-GP) were evaluated and compared as controls to ascertain the viability of geopolymer for repair application. The shear bond strength of FAGP mortar was found to be in the order of 14 MPa, outperforming OPC and P-GP in all substrate conditions. Even though FAGP bond strength was insensitive to roughened substrate moisture levels, the synergistic effect of smoothness and moisture condition appeared detrimental. The testing of the prototype geopolymer-coated concrete pipe under line loading showed no sign of delamination at the bond plane. OPC and P-GP exhibited a distinct bond separation, which commenced at only 20 % of the ultimate load. The acid resistance and low permeability of FAGP mortar appeared to aid in preserving the repair bond.

1. Introduction

Repair of concrete is a rapidly evolving discipline seeking solutions for the perpetual demand to extend the service life of functionally obsolete structures [1,2]. Concrete repairs can be in various forms, including reconnecting fractured concrete surfaces for a reliable monolithic load transfer or encapsulating a damaged concrete surface to protect it from further exposure to hostile environments [3,4]. Concrete sewer infrastructure is one of the most vulnerable and expensive schemes to repair due to exposure to aggressive corrosive environments. This is primarily due to Microbial Induced Concrete Corrosion (MICC), which causes the concrete pipe wall in the sewer setting to disintegrate when cementitious products react with biogenic sulphuric acid, reducing sewer pipe service life significantly and requiring costly repair or replacement [5,6]. Extensive pipeline mileage to serve the growing urban population and increasing sewage temperatures due to climate change have been reported to enhance the degree of damage and repair

incidence [7]. According to the Queensland Water Regional Alliance Program Research Report [8], the total length of sewers in Queensland, Australia, was 33,500 km in 2017, with a repair cost of 7.78 million AUD, excluding pipe renewals. With an optimistic replacement rate of 0.3 % each year, the estimated sewer replacement cost by 2030 is 365 million AUD, rising exponentially to 1.15 billion AUD by 2040. In response, efforts have been made to optimise cementitious formulations to resist biogenic sulphuric acid deterioration, with a greater emphasis on improving bond characteristics to overcome the poor reliability of Ordinary Portland Cement (OPC)-based repair binders at cold joints and their low microcrack resilience; however, with limited success [2,9,10]. Despite their superior acid resistance, polyurethane, epoxy resin, and acrylic polymer have also been reported to be short-lived as sewer linings due to material incompatibility with the existing concrete substrate. This property is critical to the composite's monolithic behaviour, enabling it to resist curling, delamination, cracking, spalling and other factors such as thermal expansion, elastic modulus, and shrinkage [10].

* Corresponding author.

E-mail address: allan.manalo@unisq.edu.au (A.C. Manalo).

<https://doi.org/10.1016/j.conbuildmat.2024.137927>

Received 20 November 2023; Received in revised form 6 July 2024; Accepted 14 August 2024

Available online 25 August 2024

0950-0618/© 2024 The Author(s). Published by Elsevier Ltd. This is an open access article under the CC BY license (<http://creativecommons.org/licenses/by/4.0/>).

The high cost and sustainability issues were also reported, discouraging organic repair binder use [11]. Therefore, new materials are now being explored as repair systems for OPC sewer infrastructures.

Geopolymer has piqued the scientific community's interest as a repair material for concrete because of its demonstrated OPC compatibility and high chemical resistance, durability, and sustainability [12–14]. Geopolymer has been extensively explored recently for its adherence to diverse concrete substrates [3,15,16] and repair feasibility on structural elements subjected to varying exposure conditions to avoid premature failures [17,18]. For instance, Pacheco-Torgal et al. [19] found that geopolymers have comparable bond strength to commercial repair products. Abdulrahman et al. [20] also investigated the geopolymer-rebar bond strength against rebar anchorage length and discovered that geopolymer behaves similarly to OPC concrete, confirming that existing OPC concrete models can be used to estimate FA-based geopolymer bond capacity in structural member design. In another study, Tan et al. [21] discovered negligible deterioration in metakaolin-based geopolymer repair in aggressive environments involving moisture and temperature changes and recommended higher percentages of granulated blast furnace slag (GGBFS) in the binder to prevent efflorescence-induced repair strength loss. The revolutionary repair technology using strain hardening fibre-reinforced geopolymer overlay, according to [22], protects the steel reinforcement in concrete members exposed to harsh environmental conditions. Geopolymer bond strength is influenced by various factors, including constituent materials, formulation, and substrate conditions [23]. The augmentation of the reaction product at the bond interface is critical to the improved shear bond strength; most research incorporated Calcium (Ca)-rich constituents (GGBFS, class C FA) into the FA-based geopolymers to introduce strong Calcium-Silicate-Hydrate (C-S-H) and Calcium-Aluminate-Silicate-Hydrate (C-A-S-H) linkages to the existing Sodium-Aluminate-Silicate-Hydrate (N-A-S-H) gel [15,24]. Gomaa et al. [25] reported the excellent performance of alkali-activated geopolymers in terms of bond strength, ranking them from good to average with Ca percentage. The rapid reaction process of Ca-rich geopolymers allows for room-temperature curing, providing a distinct advantage over low calcium geopolymers that necessitate energy input for curing. Geopolymers have been in the market as a coating material for concrete water pipes for nearly a decade due to their rapid setting times and enhanced structural performance under compression; shorter bypass times due to pipe repair have been reported to result in less financial losses and community disruption than OPC repairs [9]. However, Gevaudan et al. [26], Valencia-Saavedra et al. [27] and Matthieu et al. [28] reported that Ca-rich geopolymers are still susceptible to sulphuric acid attack and their efficacy as a coating material is in question to deploy in harsh sewer conditions. Tan et al. [29], Ojha and Aggarwal [30] also reported that C-A-S-H bonds are susceptible to acid attacks despite enhancing bond strength. Hence, sufficient attention to short-term and long-term durability properties is important for using low calcium geopolymers as a repair material, despite the limited focus it has received to date. Since many geopolymer findings are limited to assessing either bond strength [31,32] or durability [33,34], additional research is necessary to evaluate the potential of low calcium geopolymers for repair purposes in aggressive sewer conditions.

Moreover, the influence of the adhesion and compatibility of the repair material, as well as the existing condition of the substrate, on the efficacy and longevity of the retrofit have been affirmed [35]. In the review by Fahim Huseien et al. [15], substantial guidelines for preparing the existing concrete substrate before repair application have been produced. The significance of surface roughness in enhancing bonds has frequently been investigated and is comparatively better understood [36,37]. However, its use in sewer pipe repair is limited by the roughness levels of a typical sewer pipe, which range from smooth below the water level to moderate at the water line and high in the crown area, depending on acid corrosion intensity. Thus, a repair mortar with good binding strength at all roughness levels is required. The surface moisture

content of the concrete substrate is considered another crucial factor for the success of the bond with the repair material and remains controversial [38,39]. Some authors [32,40] propose a saturated dry surface for cementitious overlays on concrete substrates for better bonding and microstructure. Since geopolymerisation differs from cement hydration, more research is required as the above recommendations would not assist in predicting geopolymer bond strength on concrete substrates [41], particularly at different moisture conditions, which is typical in repairing sewer walls.

In addressing the above research gap, this study investigated the bond performance of low calcium FA-based geopolymer mortar. Slant shear strength tests implemented by Ganesh and Murthy [42] were conducted to quantify the overlay-substrate bond strength at different substrate conditions, simulating a typical sewer pipe wall condition. In addition, a test was devised to assess the fracture propagation and its qualitative impact on the repair interface in a lined pipe segment using the Digital Image Correlation (DIC) technique. Standard OPC and commercial geopolymer repair mortar were incorporated to compare results. The findings of this study offer insight into the feasibility of low calcium geopolymer as a repair system on concrete surfaces with diverse conditions ranging from dry to saturated and smooth to rough. Furthermore, the scope of this study could be broadened to investigate the long-term performance of geopolymer repairs in sewage environments, specifically the efficacy of low calcium geopolymer in mitigating the formation of detrimental calcium salts in the MICC process.

2. Materials and methods

2.1. Materials

Low calcium FA, ASTM Class F FA (from Queensland, Australia) was utilised as the raw material in geopolymer synthesis to limit the available free Ca^{2+} to react with acids. This type of material is used since this work is an antecedent to studies of geopolymer coating durability against biogenic sulphuric acid exposure. For comparison, OPC was used as a counterpart in this experiment; the chemical composition of these two binders determined by X-ray fluorescence (XRF) analysis is listed in Table 1. In the presence of low Ca^{2+} , SiO_2 , Al_2O_3 and Fe_2O_3 were considered the key reactive components of class F FA used in this study, as also found by Lokuge et al. [43]. According to Chen et al. [44], crystalline SiO_2 participates in geopolymerisation under specific conditions.

In geopolymer synthesis, these reactive components of FA precursor were activated by a pre-mixed alkali activator solution (AAS) composed of D-grade liquid sodium silicate (SS), 44.1 % solids by weight and reagent grade sodium hydroxide (SH) pellets diluted in tap water. Mortar mixes for GP and OPC were made with river sand of fineness modulus 2.83. The sand was not graded specifically, but the particles were ensured to be between 75 and 500 microns. In this study, three distinct alkali-activated GP mortar mixes were used, and their mix designs were chosen with a target of 30 MPa to 40 MPa of 28-day compressive strength. A commercially accessible proprietary geopolymer (P-GP) mortar spray product was also incorporated in this study for benchmarking purposes. In this investigation, a substrate with a higher stiffness than the overlay was utilised to avoid undesirable cohesion failure in the substrate during the bond strength test. To obtain a 50 MPa substrate compressive strength, a weight ratio of 1:1:2:0.4 was chosen, comprising OPC precursor, fine aggregates (river sand), coarse aggregates (maximum size 7 mm), and water. The mix proportions for substrate and repair overlays are summarised in Table 2.

2.2. OPC concrete substrate preparation

The ASTM C882 standard [45] for slant shear test was followed in preparing the OPC concrete substrate, which represents the concrete sewer pipe wall. As shown in Fig. 1, cylindrical Polyvinyl chloride (PVC)

Table 1
Chemical composition of the low-calcium fly ash binder in comparison with typical OPC.

Oxide, (wt%)	SiO ₂	Al ₂ O ₃	Fe ₂ O ₃	CaO	P ₂ O ₅	TiO ₂	MgO	K ₂ O	SO ₃	MnO	Na ₂ O	LOI *
Class F FA	47.9	28.0	14.1	3.8	1.8	2.0	0.9	0.6	0.3	0.2	0.4	0.4
Typical OPC	18.1	3.1	4.75	51.9	-	0.17	1.57	0.3	2.0	-	0.17	-

Note: LOI* - Loss of ignition at 1000 °C.

Table 2
Mix proportion of substrate and mortar overlays.

Repair Composite	Mix ID	Quantity(kg/m ³)							
		OPC	FA	SS	SH	Fine aggregate	Coarse aggregate	Extra Water	
Substrate (OPC concrete)	OPC-Sub	474	-	-	-	474	948	201	
Mortar Overlay	FA geopolymer	FAGP-1	396	171	85	754	-	1	
		FAGP-2	406	150	75	748	-	18	
		FAGP-3	329	121	61	909	-	15	
OPC	OPC	370	-	-	-	555	-	166	
Proprietary geopolymer	P-GP	1275(binder + aggregate)							169*

*As per manufacturer's specifications.

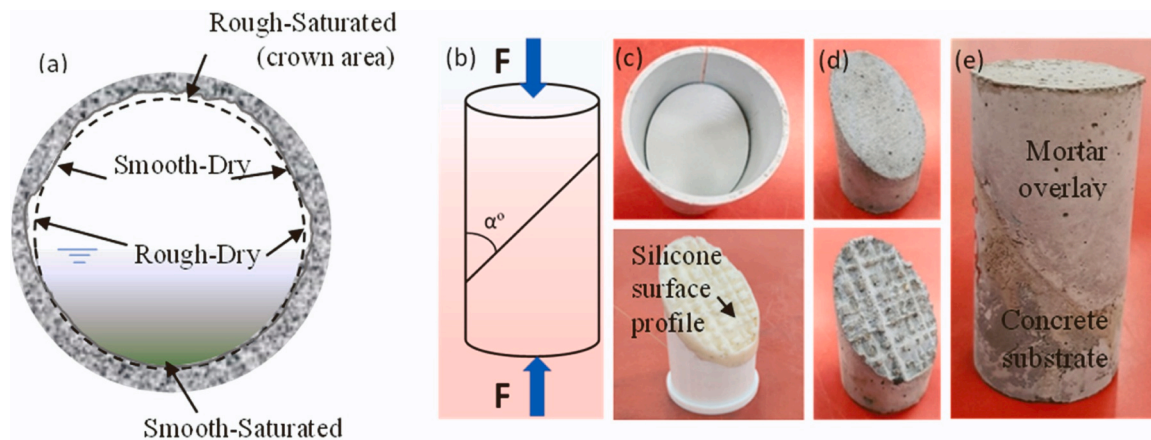


Fig. 1. – (a) Schematic diagram for different surface conditions of a sewer pipe wall, (b) slant shear test setup ($\alpha = 45^\circ$), (c) 3-D printed dummy and silicone mould, (d) prepared substrates, and (e) a prepared repair composite specimen.

moulds of 50 mm diameter and 100 mm height were used to prepare the repair composites. Despite the inclined angle (α°) for the bond plane stipulated by ASTM C882 [45] as 30° , some researchers reported that a standard 30° bond plane is incompatible with all types of substrate surface roughness states because the external stress needed to cause a shear failure along the bond interface varies with the bond angle [36, 40]. According to the Mohr-Coulomb failure criterion, the critical bond angle to produce minimal bond failure is a function of the internal friction angle, thus substrate surface roughness. Slant shear strength increases with substrate surface roughness, and material failure is more probable if the bond plane angle is wider than the critical angle. According to Austin et al. [36], $\alpha^\circ < 30$ is ideal for substrates with non-smooth surfaces to avoid distortion of test results. In contrast, Gomaa et al. [25] demonstrated that adhesion between alkali-activated material and concrete substrate material can be accurately predicted using the slant shear test at a bond angle of 45° . Thus, this study used a 45° bond plane angle (Fig. 1(b)) in addition to two other reasons. First, MICC-induced surface deterioration differs by location within the sewer pipe wall (Fig. 1(a) shows the crown area and tidal zone being most affected); adopting a common surface roughness for the substrate is, therefore, not feasible. Second, with steep bond planes, the fresh mortar fluidity (sprayable nature) of the selected overlay mixes may create varied strains along the plane due to mortar aggregate segregation.

The conventional methods of substrate synthesis for the slant shear, including cutting/sawing a full specimen into two identical halves and

surface modification by water jetting, needle gunning, grooving, sand-blasting, or sand filling, were avoided in this study due to the reported shortcomings of potential alterations in macro and micro characteristics of the material at the bond plane, thereby accelerating failure [35].

Alternatively, this work used 3D-printed surface roughness profiles where a random image of a deteriorated sewer pipe wall surface was projected onto a 3D printable shape to reproduce the substrate roughness. Silicon profile moulds, as seen in Fig. 1(c), were made from the 3D printed profile for easy removal and to avoid any substrate surface contamination from using lubricants. The produced concrete substrates (Fig. 1(d)) were demoulded 24 hours later and stored in a moisture room at $24 \pm 2^\circ\text{C}$ and 96 % humidity for 28 days, followed by an additional seven days at ambient temperatures wrapped in polythene sheet to ensure the hydration process was approaching maturity.

2.3. Simulation of substrate conditions

Before applying the repair overlay, the aged substrates were conditioned to simulate a typical sewer pipe wall. Since sewers typically function at part-flow, the moisture levels within the pipe walls vary. The subaqueous sewer walls at the bottom of the pipe are fully saturated, whilst the region above the water level is low in moisture [5]. However, in-situ investigations [7,46] have reported well-moistened sewer head-space (crown area) resulting from the condensation of water vapour and other gases volatilised at the liquid-gas interface. In the current study,

the saturated substrate condition was achieved by soaking one-half of both specimens in water for 48 hours, followed by pat drying for 2 hours. The remaining substrates were overlaid with repair mortar in dry conditions. This study investigated four distinct substrate conditions; Rough-Dry, Rough-Saturated, Smooth-Dry, and Smooth-Saturated (Fig. 1(a)). A total of 36 specimens were prepared, with each mix and substrate condition being replicated three times.

2.4. Geopolymer overlay preparation

The fresh geopolymer repair mortar was applied to the precast concrete substrate inside the cylindrical mould. Following demoulding (Fig. 1(e)), it was heat-cured for 24 hours at 80 °C before curing for an additional 27 days at ambient temperatures (24 ± 2 °C). The demoulded bonded specimens for OPC and P-GP were maintained at 24 ± 2 °C and 96 % humidity until the 28-day test date.

2.5. Test procedure and instrumentation

2.5.1. Overlay material characterisation

2.5.1.1. Flowability. The flow of fresh repair mortars was assessed per the ASTM 1437 [47] method, which measured the average diameter of mortar spread over the concentric circles of the standard flow table and computed the resultant increase in the spread as the flow, expressed as a percentage of the original base diameter.

2.5.1.2. Compressive strength. Material testing on the substrate and repair materials supplemented the bond tests. Compressive testing was performed on 50 mm × 100 mm cylinders using 100 kN capacity MTS Universal Testing equipment at a loading rate of 0.5 kN/s. The ASTM C109 [48] the standard was used to assess compressive strength; all tests were performed in triplicate, and the average results and standard deviations are reported in Fig. 3.

2.5.2. Coating performance

Slant shear testing in accordance with ASTM C882 [45] was used to evaluate the bond strength between the repair overlay and the OPC concrete substrate. The prepared concrete composites (as described in Section 2.2) were subjected to axial compressive loading at a 0.5 mm/min rate until the failure occurred. σ_0 is the vertical stress (in MPa), depicted by Eq. (1), imposed at the surface of the repair composite to cause a shear failure along the bond plane; A_0 is the area of the slanted bond plane. σ_0 also known as the bond strength by the slant shear.

$$\sigma_0 = \frac{F}{A_0} \quad (1)$$

Eqs. 2 and 3 were used to obtain shear and normal stresses at the interface for the slant shear test specimens.

$$\tau_n = \frac{1}{2}\sigma_0 \sin 2\alpha \quad (2)$$

$$\sigma_n = \sigma_0 \sin^2 \alpha \quad (3)$$

The shear and normal stresses acting on the bond plane are represented as τ_n and σ_n respectively (Eqs. 2 and 3), whereas α is the bond plane inclination from the vertical, which in this study is equal to 45°.

Based on the Mohr-Coulomb theory (Eq. 4),

$$\tau_n = C + \mu \sigma_n \quad (4)$$

Where, C and μ denote cohesion (pure shear) and surface friction coefficient, respectively.

2.5.3. Acid exposure and strain mapping with DIC

Testing a repaired element in relevant application scenarios is

critical for evaluating the composite properties. Fig. 2(a) depicts the ring deflection diagram for a pipe under a line load, a typical test setup for a subterranean sewer pipe. However, assessing the fractures at a given load or at the failure load does not suffice; monitoring fracture genesis and propagation by measuring field stain is critical to understanding the repair impact, which is still poorly understood in assessing in situ pipe repair liners.

The use of strain maps in the assessment of restored structural components in service scenarios, such as a repaired sewer pipe [17], provides significant information about probable future failures caused by inadequate bonding regions or anomalies in the repair substance. To simulate this, concrete pipe segments (125 mm internal diameter with 25 mm thickness) were manufactured as shown in Fig. 2, in accordance with the ASTM F2551-09 [49] requirements for installing a protective liner in sanitary sewers. These concrete pipes were coated with repair mortars (8 mm thickness), namely FAGP-1, OPC, and P-GP, at the saturated surface dry condition, as illustrated in Fig. 2(b). After 28 days of curing, the coated pipe segments were exposed to 0.5 pH sulphuric acid for a duration of 1000 hours in a part-full state as displayed in Fig. 2 (c) and (d). The pipe segments were subsequently loaded in accordance with the AS/NZS 4058:2007 [50], employing a two-edge bearing test as depicted in Fig. 2(e). The load was applied in a direction parallel to the vertical centreline of the pipe, along the specimen, at a controlled rate of 0.2 kN/s. Gravity sewers were the focus of this study, and they are designed as part-full, with low internal pressure compared to external loads. Assuming equal lateral soil pressures, an underground pipe experiences vertical pressure, exerted mostly above its crown as a function of soil cover, infrastructure, and axel loads. This investigation is confined to a comparison of different types of mortar. Consequently, this research examines the impacts of axial load on the pipe segment, specifically the generation of bending stresses at the crown, invert, and streamlines to permit bending-shear at the bond plane (Fig. 2(a)). This study did not evaluate internal and exterior loads caused by soil bedding and flow, nor the associated stresses that occur in real-life conditions. To evaluate stresses due to acid attack and the subsequent fracture propagation at the bond contact qualitatively, the strain distribution of the ring area was photographically recorded and then analysed by the DIC method explained by Liu et al. [51]. DIC is an optical approach renowned for its robustness and versatility in assessing material properties such as strain, elasticity and shape deformation achieved by meticulous analysis of images [52]. Before the DIC test, the surface area along the pipe perimeter was cleaned and sprayed with black paint to easily create a speckle pattern, which is ideal for precise displacement and strain measurement. The images were captured using a camera at a speed of 10 Hz, followed by processing using the GOM correlation software tool, where the strain field is calculated using the established correlation criterion between the reference and distorted images. The full-field strain maps obtained at the specified timings were utilised to identify the fracture initiation and delamination of the repair bond; details are in Section 4.

Based on Fig. 2(a), slippage of layers and debonding (ϵ_{slip}) are caused by strain differences between the substrate (ϵ_s) and the mortar (ϵ_m); this relationship is depicted by Eq. (5). If fully bonded, there is no potential for slippage at the bond interface (Eq. 6).

$$|\epsilon_{slip}| = \epsilon_s - \epsilon_m \quad (5)$$

$$|\epsilon_{slip}| \cong 0 \quad (6)$$

3. Results and discussion

3.1. Flow and compressive strength of repair mortar

Fig. 3 illustrates the flow characteristics and 28-day compressive strength of repair mortars and the substrate concrete used in this study. According to the flow measurement, the fresh FAGP-2 flow was

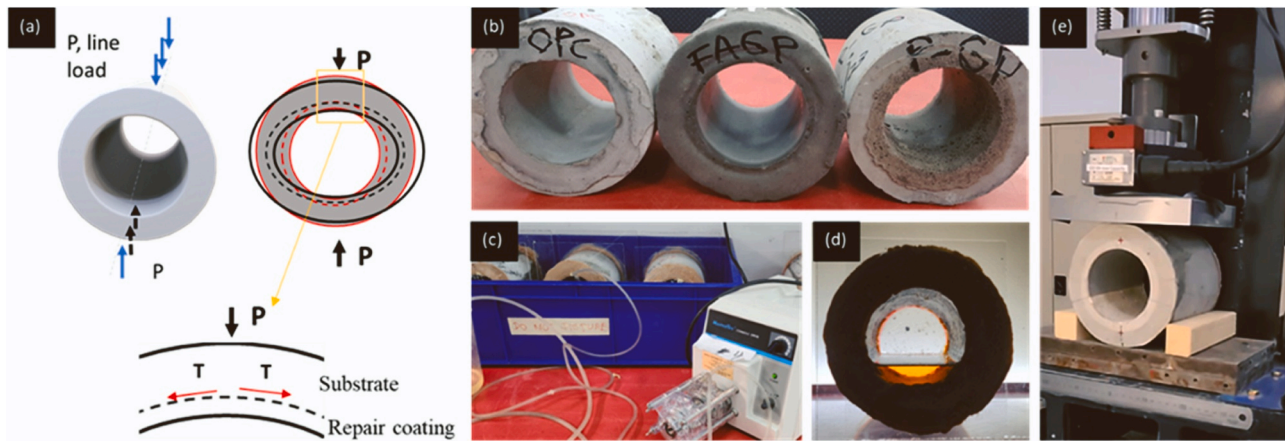


Fig. 2. – (a) Ring deflection set-up for a pipe under a line load, (b) concrete pipe segments lined with repair binders, (c) experimental set up for aggressive H₂SO₄ acid exposure, (d) P-GP mortar-lined pipe after 1000 hrs of acid exposure, and (e) a pipe segment under loading.

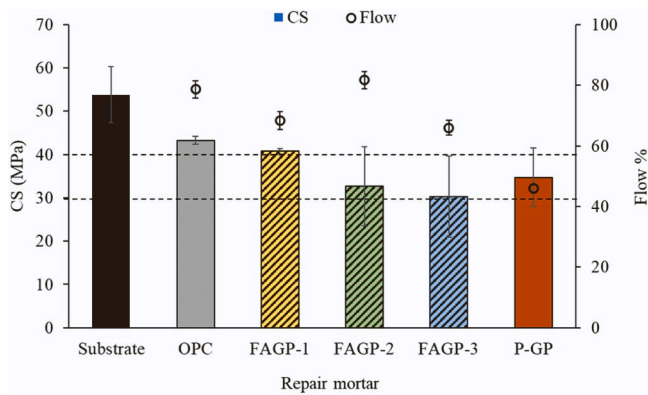


Fig. 3. – Results for flow value of fresh repair mortars and 28-day compressive strength.

equivalent to OPC mortar (around 80 % flow), whilst the flow values for other FAGP were within the 60–80 % range and were observed as satisfactory workability (neither very dry nor self-compacting). A flow consistency of 80 %–90 % was optimal for the vertical pouring of the mortar liner without fine aggregate segregation. Compared to the P-GP, it showed the lowest flow of all, which was 46 %. As can be seen from the compressive strength results, conventional concrete sewers have a compressive strength of 45–50 MPa. However, this study sought a higher strength (>50 MPa) for substrate concrete to distinguish failure modes/patterns. The mechanical strength properties of the mortars differed as expected, which is reflected in Fig. 3. The compressive strength of FAGP-1 was the highest compared to the other geopolymer repair mortars, and it was 40 MPa, equivalent to OPC repair mortar. The compressive strength of the remaining three geopolymer mortar mixes, including the commercial geopolymer, was lower and in the 30–35 MPa range. The strength increases in FAGP-1 compared to other types of FAGP geopolymer is attributed to the higher activator content in the mix. This aided in accelerating the geopolymerisation reaction, resulting in higher strength than the other two types.

3.2. Bonding strength between the mortar overlay and OPC concrete substrate

The shear bond strength of repair mortars was evaluated under various combinations of substrate settings; slant shear test results and failure mode details are given in Table 3. A, A-S, O-S, and S are the most prevalent failure modes detected and stand for Axial split, Axial split-shear combined, Overlay-Shear combined, and Shear only,

Table 3
Slant shear test results for repair mortars at varying substrate conditions.

Specimen ID	Substrate condition	σ_c (MPa)	STD	Average failure mode	Minimum shear bond strength (MPa)
FAGP-1	Rough- Dry	5.86	1.03	Axial split (A)	5.86
	Rough- Saturated	5.03	0.19	Axial split + shear (A-S)	5.03
	Smooth- Dry	5.58	0.77	A	5.58
	Smooth- Saturated	4.82	0.32	A-S	4.82
FAGP-2	Rough- Dry	5.70	0.85	A	5.70
	Rough- Saturated	4.72	0.43	A-S	4.72
	Smooth- Dry	4.62	0.67	A-S	4.62
	Smooth- Saturated	4.44	0.10	A	4.44
FAGP-3	Rough- Dry	4.38	0.29	A	4.38
	Rough- Saturated	4.30	0.34	A-S	4.30
	Smooth- Dry	3.44	0.34	A-S	3.44
	Smooth- Saturated	3.09	0.23	A-S	3.09
OPC	Rough- Dry	6.46	0.25	Overlay material +Shear (O+S)	6.46
	Rough- Saturated	7.95	0.48	O-S	7.95
	Smooth- Dry	6.15	0.92	Shear only (S)	6.15
P-GP	Smooth- Saturated	7.57	0.34	S	7.57
	Rough- Dry	5.49	0.77	O-S	5.49
	Rough- Saturated	6.15	0.67	O-S	6.19
	Smooth- Dry	4.89	0.40	S	4.89
	Smooth- Saturated	6.54	1.07	S	6.54

respectively, as shown in Table 3. The minimum bond strength for repair, as stipulated by ASTM C882, is the slant shear stress at the point of failure [19]. The minimal bond strength has been adopted as the actual bond strength for cases where the failure occurred exclusively at the bond interface (a shear failure). Although interface roughness and specimen geometry influence slant shear strength, distinguishing bond characteristics between repair materials prepared and evaluated under the same conditions is advantageous [53]. Fig. 4 depicts the minimum

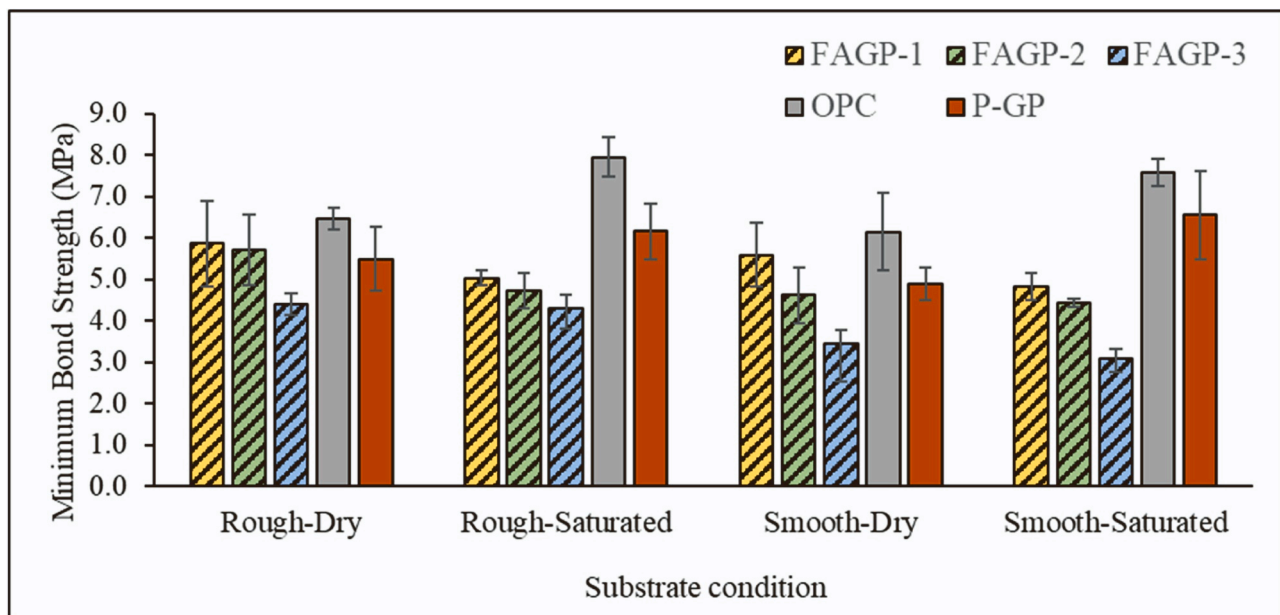


Fig. 4. – Comparison of minimum shear bond strength between repair mortars at substrates with different surface roughness and moisture levels.

bond strength of each mortar at various substrate conditions. Mortar bond strength results and the corresponding failures are discussed in detail below.

3.2.1. Rough - dry

As depicted in Table 3, composites with geopolymer overlay showed monolithic failure for all geopolymer repair mixes and reached an average slant shear bond strength of 5.86 MPa, 5.7 MPa and 4.38 MPa for FAGP-1, FAGP-2, and FAGP-3, respectively. The cracks propagated led to vertical splits in each geopolymer repair, indicating a strongly bonded interface with increased roughness levels in the substrate. This can be attributed to interfacial tortuosity, which affects the effective contact area of the substrate-repair mortar, which benefits the interlocking actions at the interfacial transition zone [35]. The flowability of the fresh geopolymer repair mortars likely facilitated this process by enabling effective permeation into cavities within the substrate profile, consequently reducing the occurrence of unbonded pockets [25]. However, the findings of this slant-shear test for geopolymer repair failed to accurately assess the actual bond strength due to the occurrence of a different failure mode than the anticipated bond failure. Instead, they produced lower bound estimations of the geopolymer-OPC substrate bond strength. This minimum shear bond strength of the geopolymer repairs was proportional to the repair material strength. The failure pattern of OPC was shown to be distinct from that of geopolymer binders, with the majority of OPC composites with Rough-Dry substrates exhibiting a combination of overlay material and shear failure; the average minimum bond strength for OPC repairs was 6.46 MPa. The cracks formed were confined to the repair overlay, indicating a stronger substrate. P-GP repairs on Rough-Dry substrates demonstrated a failure pattern similar to OPC, with equivalent minimum bond strength with FAGP-1 and FAGP-2. Cracks manifested along the bond plane within the overlay, culminating in material failure and bond separation. Larger aggregate particles and reduced flowability may cause fresh P-GP mortar limit entering coarsened substrate cavities, lowering the bonded area, and weakening the bond.

3.2.2. Rough- saturated

The rough-saturated substrate condition used in this investigation resembles the crown section of the sewer pipe wall (Fig. 1), which has the highest biogenic acid corrosion; because water vapour and gaseous

H₂S condense in the crown area, it is typically moist and degraded. Under saturated conditions, OPC repair demonstrated enhanced slant shear bond strength of 23 % compared to repairs at Rough-Dry substrate conditions. This behaviour is well documented and attributed to the completion of OPC overlay cement hydration in excess substrate moisture, resulting in improved performance and bond strength. Studies by AlHallaq et al. [39] proved that the moisture degree of the substrate has an impact on the bond strength of concrete and it is more significant in High Strength Concrete (HSC) than Normal Strength Concrete (NSC). This was opposed by Bentz et al. [31]. They discovered that dry substrates induce significant microstructural changes at the OPC repair mortar-substrate interface, drawing moisture from the fresh repair mortar and densifying the overlay adjacent to the bond plane, resulting in higher shear strength. However, when assessing the efficacy of geopolymer repair on similar surface conditions, it was discovered that the slant shear stress at the composite failure was detrimental compared to the Dry-Rough condition. According to Ahmad Zailani et al. [54], this is owing to the new cross-link bonds formed between the OPC substrate and the fresh FA-based geopolymer during the production of C-A-S-H gel by integrating free Ca⁺² cations from the OPC substrate's surface, where excess moisture negatively affects the process. The failure patterns observed in the geopolymer repairs confirmed this scenario, as all three geopolymer mortars displayed similar combined axial split and shear failure behaviour. The geopolymer mortar with the highest alkaline activator-to-FA binder ratio (FAGP-1) demonstrated the highest slant shear strength regardless of the substrate wetting condition; this clearly explains the formation of strong bonds at the Interfacial Transition Zone (ITZ) in the medium of an abundance of Na⁺ ions with reduced free water. However, identifying the novel geopolymeric phases formed at the bond interface and linking them with bond strength data necessitates additional microstructural evolution research. Moreover, P-GP repairs showed potential to improve bond strength on a saturated substrate, but the gain was negligible compared to OPC repairs. Cracks were observed in all three P-GP repair replicates that developed in the overlay and migrated to the bond plane, creating localised strains at the ITZ before failure. The failure mode for OPC was similar to P-GP and involved overlay and shear failure.

3.2.3. Smooth- dry

Table 3 depicts the slant-shear test results for FAGPs, OPC, and P-GP

mortar overlays on Smooth-Dry concrete surfaces. Since the substrate is a smooth surface, the repair bond is predominantly governed by its adhesive component [36]. Interfacial bond failure was seen in all three replicates of OPC repairs (Table 4), with an average shear bond strength of 6.15 MPa. P-GP repairs, like OPC, displayed complete shear failure at the bond plane with a shear bond strength of 4.89 MPa, which is 20 % lower than the shear bond strength of OPC at Smooth-Dry substrate condition. In contrast, FAGP repairs, as shown in Table 4, experienced axial split failure at the overlay-substrate plane; hence, the resulting slant shear strength values cannot accurately represent the shear bond strength, rendering any s with other repair mortars unreliable. The reported minimum bond strength for geopolymers was slightly reduced compared to the rough substrate in a dry state. However, the FAGP-1 mix ($\sigma_o = 5.58$ MPa) appears to be higher than the P-GP bond strength and only 9 % lower than the OPC counterpart, confirming a high interfacial bond strength between geopolymer and OPC concrete. The particle size distribution of the aggregate in use and the binder material characteristics, size, and amount of fibre contained in the GP-P repair overlay may significantly influence its bond strength; however, these factors were not included in the shear bond strength comparison.

3.2.4. Smooth- saturated

OPC and P-GP repairs have shown increased shear bond strength at

saturated substrate conditions over the dry condition, and the values were 7.57 MPa and 6.54 MPa, respectively. It is obvious that the properties of cementitious repair bonds are enhanced with the presence of moisture, as also found in Daneshvar et al. [40]. Geopolymer bonds appeared to be impaired on Smooth-Saturated concrete substrate, as seen in Rough-Saturated circumstances, indicating that an insufficient amount of Ca^{+2} in the binder systems impedes the completion of C-A-S-H gel formation. When overlaid over a Smooth-Saturated concrete substrate, all FAGP mortar mixes had the lowest result for minimum shear bond strength. Since the failure pattern of these specimens was classified as A-S, the slant shear stress at the failure was considered as the minimum shear bond strength, which was 4.82 MPa, 4.44 MPa, and 3.09 MPa for FAGP-1, FAGP-2, and FAGP-3, respectively (Table 3).

3.2.5. Repair composites with reduced bond area

A reduced bond area was introduced on the same bond plane to promote shear bond failure and the resultant slant shear test values are tabulated in Table 5. The modified bond plane was defined as an elliptical shape, with its length and width being half the dimensions of the original elliptical bond plane, depicted in Fig. 5(a). Before applying the repair mortar, the remaining surface of the substrate was covered with a heavy-duty waterproof sticker paper to isolate the area to be bonded. Fig. 5(b), (c), (d), and (e) depict the shear failures of representative

Table 4 Failure patterns of slant shear test composites.













Repair Binder	Substrate Condition			
	Rough-Dry	Rough-Saturated	Smooth- Dry	Smooth-Saturated
FAGP-1	 A- Failure	 A+S Failure	 A- Failure	 A- Failure
OPC	 O+S Failure	 O+S Failure	 S- Failure	 S- Failure
P-GP	 O+S Failure	 O+S Failure	 S- Failure	 S- Failure

Table 5

Shear bond strength results for FAGP-1 and OPC mortars at a reduced area of bond surface.

Specimen ID	Substrate condition	σ_o (MPa)	STD	Failure mode	Shear bond strength (MPa)
FAGP-1	Rough- Dry	14.84	0.23	S	14.84
	Rough- Saturated	13.52	0.61	S	13.52
	Smooth- Dry	14.04	0.48	S	14.04
	Smooth- Saturated	13.29	0.35	S	13.29
OPC	Rough- Dry	8.20	1.1	S	8.20
	Rough- Saturated	10.0	0.35	S	10.0
	Smooth- Saturated				

FAGP specimens manufactured at Rough-Dry, Rough-Saturated, Smooth-Dry, and Smooth-Saturated conditions. For comparison, geopolymer mortars with the highest predictive bond strength, i.e. FAGP-1 mortar against OPC, were used and it clearly shows that the shear bond strength of FAGP -1 mortar outperformed OPC, repaired at all possible substrate conditions at a sewer pipe wall confirming its viability as a repair mortar for sewer rehabilitation. The maximum slant shear bond strength reported for FAGP-1 was 14.84 MPa at Rough-Dry substrate conditions, comparable to the bond strength of Ultra high-performance concrete (UHPC) tested by Al-Madani et al. [55]. Shear was the predominant failure mechanism observed in Rough-Dry specimens. Substrate cracking, conversely, indicates that the actual bond strength may be higher than the measured value, demonstrating a strong bond between the FAGP and the Rough-Dry concrete interface (Fig. 5(b)). FAGP-1 mortar on Rough-Saturated (Fig. 5(c)) and Smooth-Dry [Fig. 5 (d)] substrates exhibited shear failure-induced scouring. In contrast, an overlay residue was seen on the Smooth-Saturated substrate (Figure (e)), indicating a weaker bond interface than under previous conditions. The lowest reported FAGP-1 bond strength was 13.29 MPa and is if repaired at Smooth-Saturated surface (area below the water level). This is similar to the values reported by Zailani et al. [56] for FA geopolymer paste on concrete substrate. Fig. 6 compares the slant shear bond strength results from this study (represented by a triangle) with previously published data. According to Fig. 6. Low calcium FA-based geopolymer (FAGP-1) is comparable to high calcium geopolymers and outperforms OPC-based repair overlays. However, assessing the FAGP repair performance in service scenarios is crucial in evaluating the repair performance, which is discussed in Section 3.3.

- (1) P-GP – Current Study
- (2) Geopolymer with Class F FA [25]
- (3) OPC – Current Study
- (4) FAGP-1 Current Study
- (5) OPC [57]
- (6) Geopolymer (High Ca FA + OPC + 10 M NaOH) [57]
- (7) Geopolymer (High Ca FA + OPC + 14 M NaOH) [57]
- (8) Geopolymer paste (FA+GBFS) [16]

- (9) Geopolymer (Class F FA) [16]
- (10) Geopolymer [19,25]
- (11) OPC [54,58], Geopolymer [54]
- (12) Geopolymer (Metakaolin) [17]

3.2.6. Results of statistical analysis

A comprehensive One-way Analysis of Variance (ANOVA) test was performed using IBM SPSS Statistics software to determine where there is a statistically significant difference in FAGP-1 bond strength between the different substrate conditions. Following that, a pairwise comparison for FAGP-1 mortar bond strength was conducted using a post-hoc Tukey HSD test, with the findings shown in Table 6.

The results revealed a significant statistical difference in binding strength when FAGP mortar is overlaid on a Rough-Dry substrate condition as opposed to a Smooth-Saturated substrate condition. When overlaid on identical surface roughness conditions, the moisture level (used in the current study) at the substrate appeared to be irrelevant to the geopolymer-concrete shear bond strength. This might be attributed to the heat-curing process, which reduces the excess moisture that could hinder geopolymerisation. Another potential factor discussed by Zhu et al. [9] in their review, involves a moderate interface bond that promotes the splitting of microcracks from the stiff repair material into the composite interface, consequently minimising shear forces generated by compression. According to Shen et al. [59], the greater the substrate’s interfacial roughness, the less influence hydrophilicity has on bonding strength. A correlation between microstructural and phase change analysis for bond evolution must be established to prove this, which is outside the scope of this work. However, the synergistic effect of the surface roughness and the saturation level does seem to influence the geopolymer-concrete bond strength. Therefore, as part of the substrate preparation for geopolymer mortar lining, a thorough cleaning of the sewer pipe, particularly the smooth surface under the waterline is proposed, not only to remove the slimy layers but also to increase the

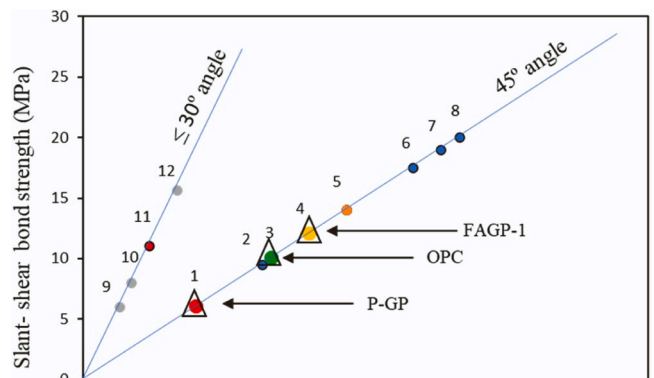


Fig. 6. – Comparison of slant shear bond strength results between published data and the current study.

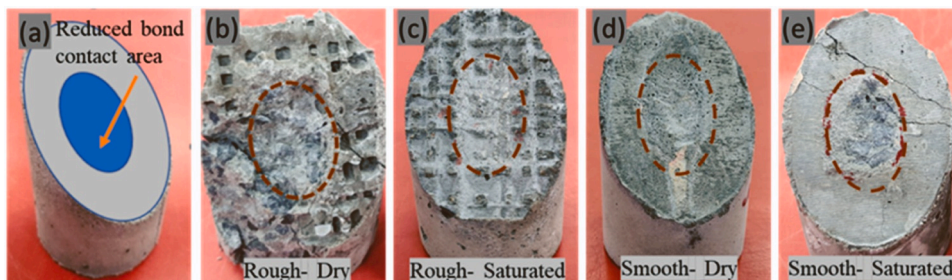


Fig. 5. – Shear failure seen in representative FAGP-1 specimens with (a) reduced bond contact area; substrates at (b) Rough- Dry, (c) Rough-Saturated, (d) Smooth-Dry, and (e) Smooth-Saturated.

Table 6
Results of post-hoc Tukey HSD analysis.

Multiple Comparisons						
Dependent variable: Slant shear bond strength (MPa)						
Tukey HSD						
(I) Substrate condition	(J) Substrate condition	Mean Difference (I-J)	Std. Error	Sig.	95 % Confidence Interval	
					Lower Bound	Upper Bound
Rough-Dry	Rough-Saturated	1.32000	0.44000	0.067	-0.0890	2.7290
	Smooth-Dry	0.80000	0.44000	0.332	-0.6090	2.2090
	Smooth-Saturated	1.55333*	0.44000	0.032	0.1443	2.9624
Rough-Saturated	Rough-Dry	-1.32000	0.44000	0.067	-2.7290	0.0890
	Smooth-Dry	-0.52000	0.44000	0.654	-1.9290	0.8890
	Smooth-Saturated	0.23333	0.44000	0.949	-1.1757	1.6424
Smooth-Dry	Rough-Dry	-0.80000	0.44000	0.332	-2.2090	0.6090
	Rough-Saturated	0.52000	0.44000	0.654	-0.8890	1.9290
	Smooth-Saturated	0.75333	0.44000	0.378	-0.6557	2.1624
Smooth-Saturated	Rough-Dry	-1.55333*	0.44000	0.032	-2.9624	-0.1443
	Rough-Saturated	-0.23333	0.44000	0.949	-1.6424	1.1757
	Smooth-Dry	-0.75333	0.44000	0.378	-2.1624	0.6557

*The mean difference is significant at the 0.05 level.

roughness. It is also important to prevent active infiltration during the geopolymer repair mortar application and curing time. This improves the adherence of the substrate and coating material, which influences the durability of the restored pipe [9].

4. Strain mapping and fracture analysis of acid-deteriorated composite specimens using DIC method

Fig. 7 shows the load- deflection-time curves alongside failure patterns of the repair mortar-coated composite specimens. The failure loads for FAGP-1, OPC and P-GP specimens were 9.22 kN, 7.63 kN and 9.97 kN at the deflection of 1.04 mm, 1.74 mm, and 2.38 mm, respectively. All specimens developed obvious fractures in the tension areas of the vertical plane (below the neutral axis) and transverse plane (above the neutral axis), typical of an unreinforced concrete pipe under a two-edge bearing load. However, as seen in Fig. 7(b) and (c), the cracks in both OPC and P-GP have propagated along the bond interface, indicating a sign of debonding of the repair layer from the concrete substrate. This can be due to either poor bonding or shrinkage-induced stresses, which caused the bond failure at the ITZ. However, no evaluations were made to assess the inherent shrinkage properties of the materials in this study. It is advantageous to analyse the stresses at the bond interface to correlate the failure load with deflection and fracture behaviour. In response, full-field strain distribution maps were employed to establish the highly stressed areas at the bonding zone; maps were acquired at various stages, from crack initiation to failure, using the DIC technique. Visual representations of individual segments of mortar-coated concrete pipes following the acid treatment are depicted in Fig. 7. The strain maps were also anticipated to demonstrate the impact of acid degradation on the bonded region.

Fig. 8 to 10 show the full-field strain distribution maps of FAGP-1, OPC, and P-GP at different stages during the test. In the x and y directions, strain is designated by ϵ_x and ϵ_y , respectively. These strains represent the axial and circumferential strains, respectively. Subscripts S1, S2, S3 and S4 are appended to differentiate the corresponding stages from start to failure (shown in Fig. 7). The S1 stage, which is common to all types of mortar, consists of strain maps collected five seconds after the test begins and used as a reference point for comparing the strain developed during subsequent stages. The initial occurrence of crack formation is denoted as S2, while S3 represents the point at which failure occurs in the coating material or the onset of debonding between the repair and the substrate. S4, on the other hand, corresponds to the time of specimen failure. Fig. 8(S1) depicts the full-field strain maps of FAGP-1 in the x and y directions, captured five seconds after the test commenced (S1). It is evident that at S1, the ϵ_x within the full-field is

considerably low ($< 0.2\%$ in both tension and compression) and was mostly evenly distributed, with the exception of a few patches of strains, S1- ϵ_x ranging from 0.4% to 0.66%. The corresponding ϵ in the y-direction showed scattered strain patches at the top and bottom sides of the ring surface along the axial loading plane at a value of S1- $\epsilon_y = 0.3\%$. In Fig. 8(S2), an initiation of cracks can be seen on the repair coating at both crown and base areas at the load of 7.43 kN and 0.91 mm deflection. At S2, the maximum strain reported in the x and y directions was 1.57% and 0.76%, respectively. As seen in Fig. 8(S3), increasing the load leads to increased ϵ_x (up to 1.83%), causing vertical crack propagation. A transverse crack in the concrete substrate was observed in S3, five seconds before failure. Despite the presence of dispersed patches of compressive strain around the bond zone, no evidence of debonding was observed at the ITZ. In Fig. 8(S4), the strain maps at the point of failure are depicted.

It is observed that there are no discernible strain variations or micro-cracks along the bond line, except for the prominent splits in the tension regions of the repair composite surface. This observation corroborates with the slant shear test results that the bond strength between geopolymer, and concrete is substantial despite a Smooth-Saturated substrate condition. The influence of acid exposure on the coating material or the bond zone is also not apparent in the FAGP strain maps, confirming FAGP's acid resistivity and lower permeability in transporting chemical compounds into the repair layer and beyond.

Fig. 9(S1) to (S4) show full-field strain maps of an OPC-based repair composite. Surface strain measurements obtained for OPC-coated concrete pipe shortly after the test began revealed similar behaviour to FAGP. However, the crack initiation (at S2) in OPC occurred at a lower load of 2.15 kN and earlier compared to FAGP, as seen in Fig. 9(S2), the cracks are localised in the bond zone with a maximum of 0.68% strain in the x direction. Furthermore, an area of S2- ϵ_x between 0.30% and 0.45% along the bond line indicated increased regional stress. The strain in the y direction was mostly oxalating between -0.4% and 0.4%. Full-field strain maps acquired 10 seconds before the failure (Fig. 9(S3)) verified the presence of transverse splits and delamination in the crown area at the bond line. The x-direction strain in the remaining region along the bond line increased to 28.9%, suggesting the repair mortar layer may detach from the concrete pipe, which scenario was not encountered in the FAGP composite. The S3- ϵ_y data indicates that the surface is mostly strain neutral, with increased positive strain at the bond zone. Although obvious to the naked eye [as seen in Fig. 7(b)], there was inadequate strain-based qualitative evidence to explain the impact of acid-induced corrosion on the OPC repair liner and bond zone. Despite OPC's susceptibility to H_2SO_4 acid attacks, the relatively low permeability of OPC may have prevented acid from reaching its deeper

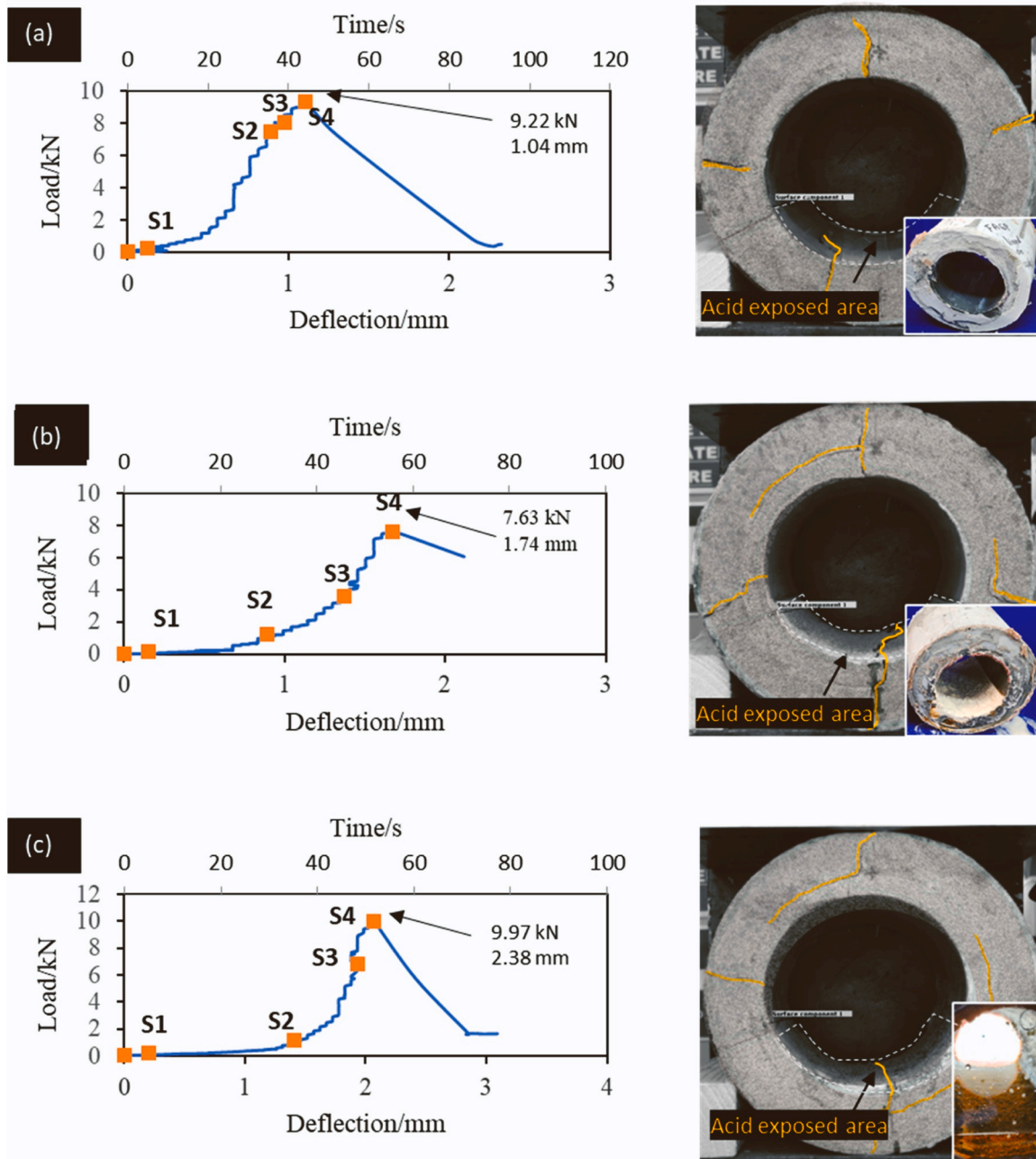


Fig. 7. – Load- deflection-time curves alongside with failure patterns of the repair mortar-coated composite specimens; (a) FAGP-1, (b) OPC, and (c) P-GP.

layers. More research on the evolution of phase shifts and corrosion products versus acid intrusion depth is proposed to support this hypothesis. Fig. 9(S4) illustrates the strain at failure, it is lower than stage S3 in both directions due to continuation of splitting and delamination.

P-GP-coated concrete pipe full-field strain distribution maps are shown in Fig. 10. Like FAGP and OPC, this study considers phases S1 to S4. S1 records the x and y strain maps as the reference 5 seconds after the test began. Both x and y were strain-neutral at S1. S2, the crack initialisation stage, began 30 seconds after the test began, later than OPC but earlier than FAGP’s first crack. Compared to OPC, the strain levels of the P-GP repaired surface at the crack initiation stage were lower and -1.5 – 2.77 % and -3 – 2.6 % in the x and y directions, respectively. However, strain along the bond plane was apparent and ranged from $\epsilon_x = 0.25$ %– 0.5 %. At stage S3, the debonding of the overlay was detected, and it was after 8 seconds from S2. The delamination initiated at the bond plane at the pipe’s bottom and propagated towards the

crown area. This can be attributed to acid permeation into the bond plane producing bond failure before repair material failure. Notably, this failure pattern differed from the similar stage S3 failure pattern observed for OPC. The recorded load value for P-GP at S3 was 6.78 kN, twice as high as the stated load value for OPC. Fig. 10 (S4) shows the full-field strain maps of a P-GP lined pipe at failure (at 9.97 kN), where ϵ_x and ϵ_y were comparable to OPC at the time of failure.

5. Conclusion

Low calcium fly ash-based geopolymer mortars were investigated for bond strength on concrete substrates with varying roughness and moisture conditions. They were compared to standard OPC and P-GP mortar to evaluate the suitability of this new repair material for application in sewer rehabilitation projects. In addition, a qualitative study of the geopolymer mortar bond performance was carried out on a

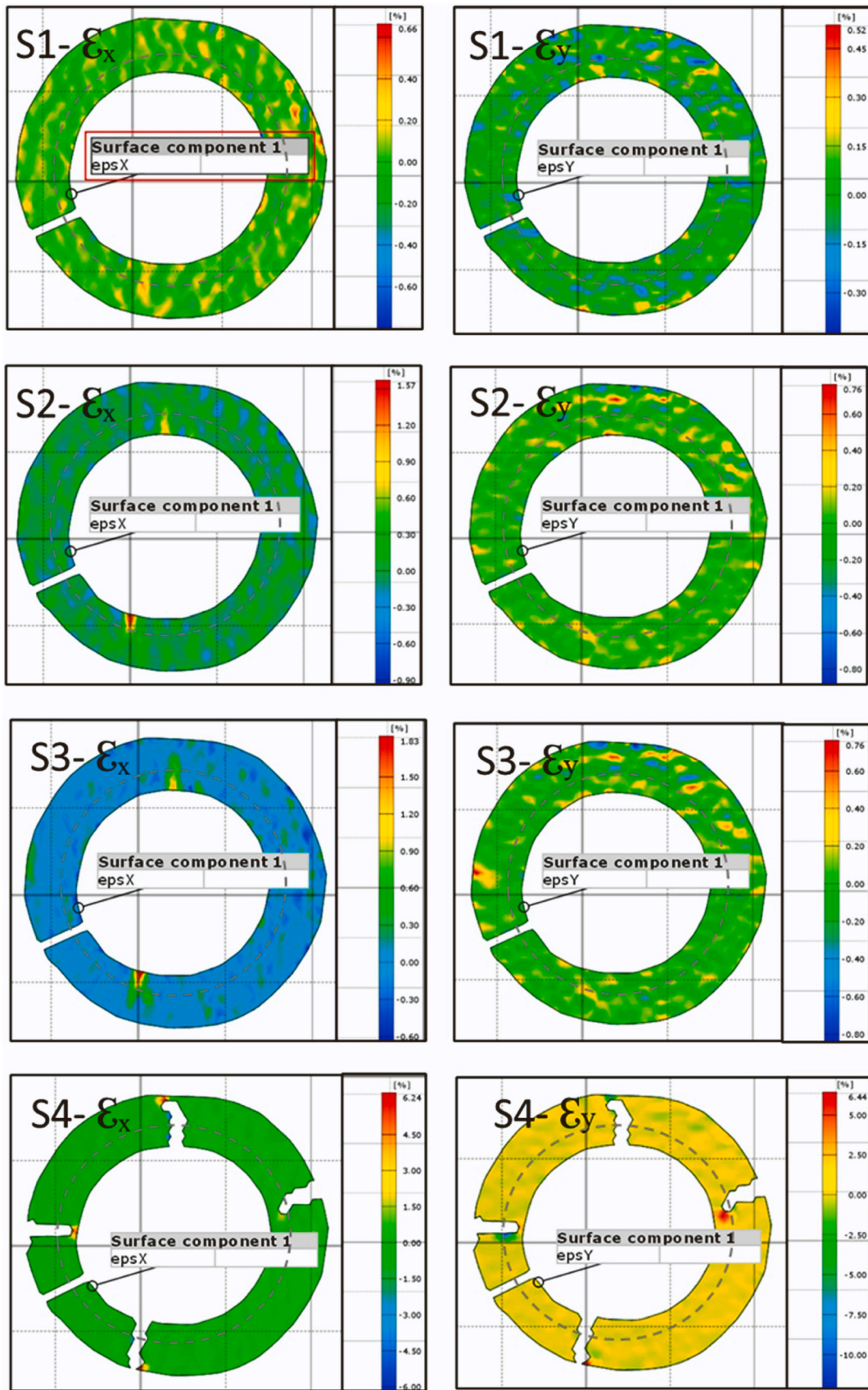


Fig. 8. – Full-field strain distribution maps of FAGP-1, at different stages during the test.

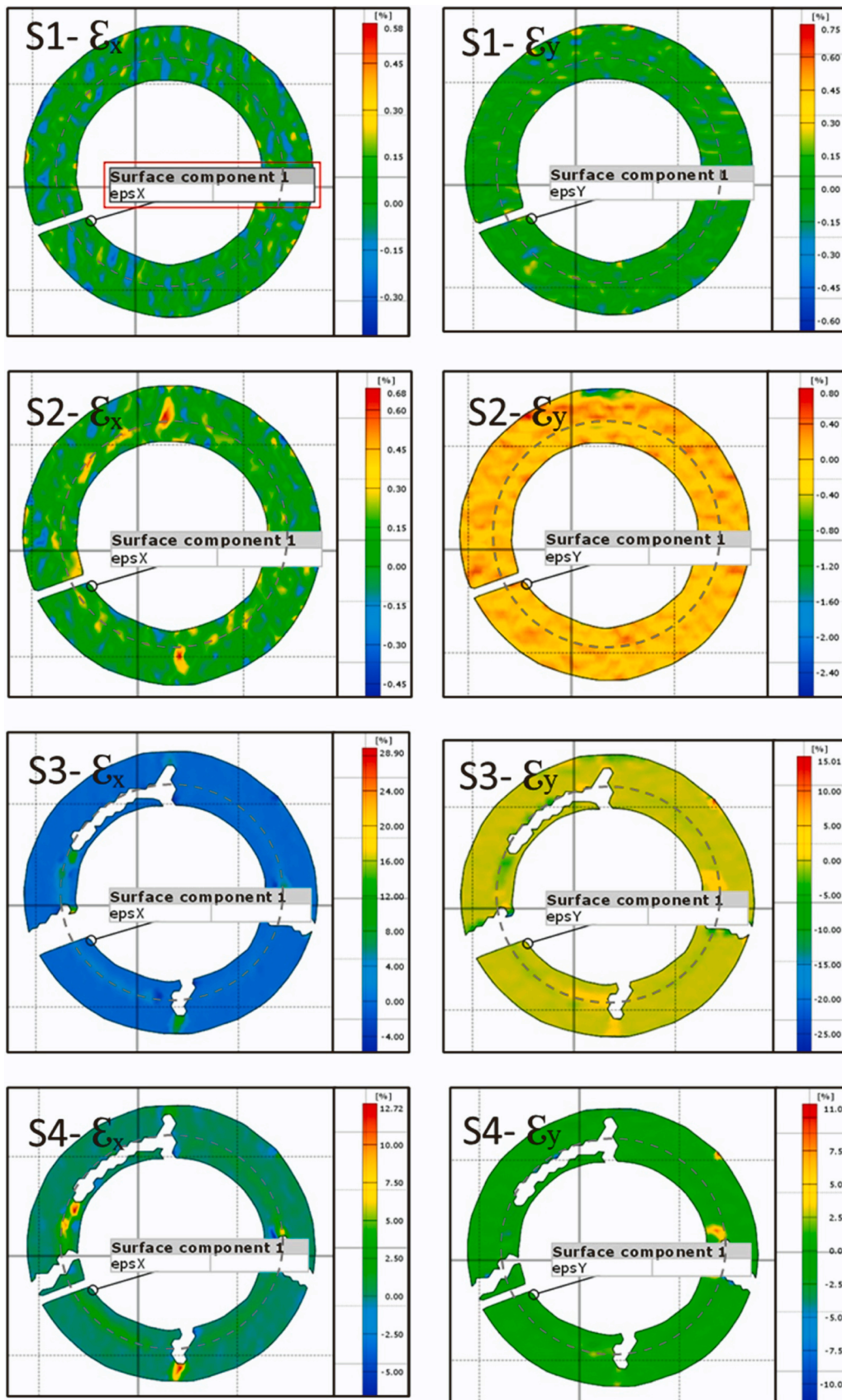


Fig. 9. – Full-field strain distribution maps of OPC, at different stages during the test.

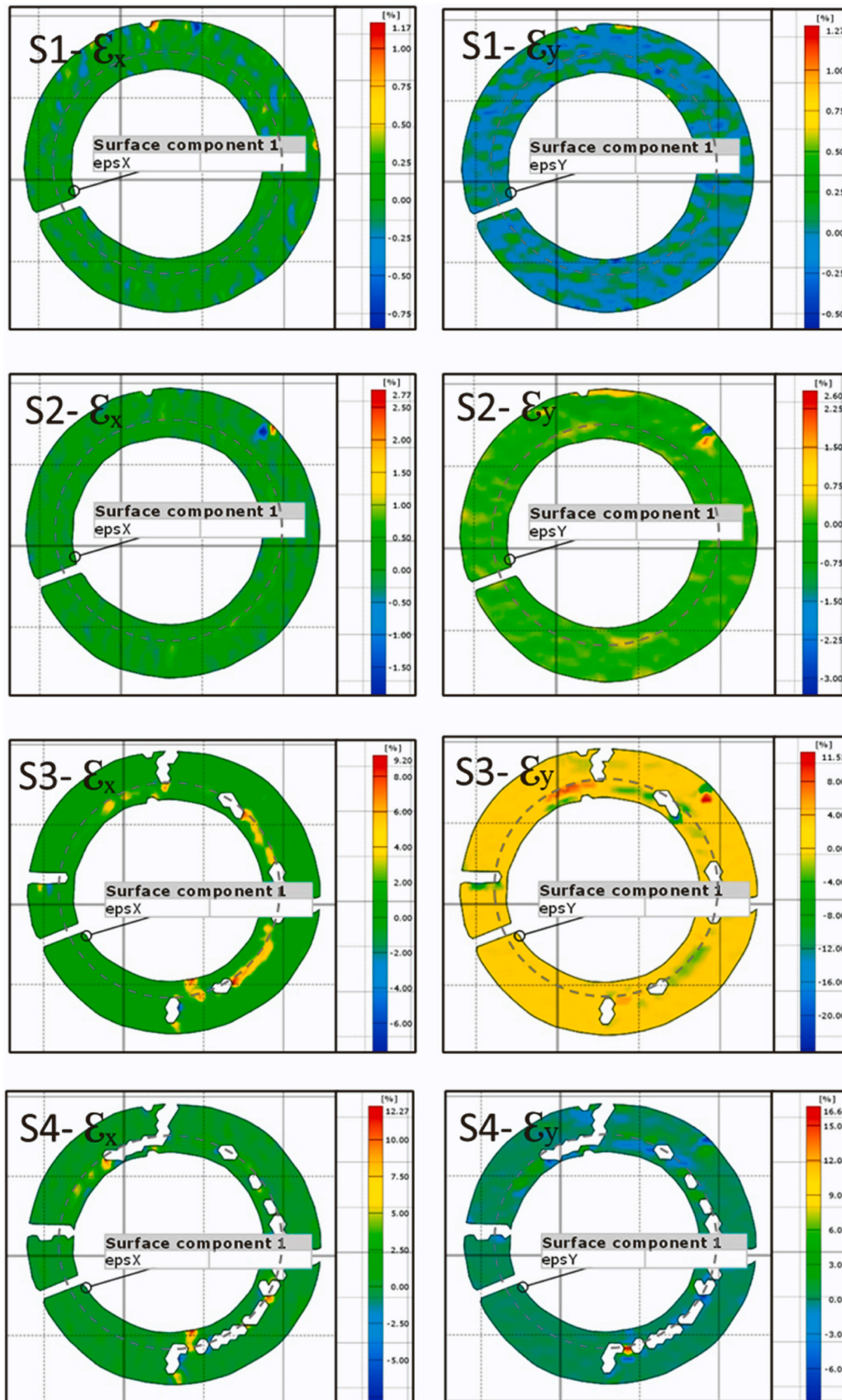


Fig. 10. – Full-field strain distribution maps of P-GP, at different stages during the test.

prototype of a mortar-lined concrete segment exposed to acid corrosion using full-field strain mapping. The following conclusions can be drawn from the results of this study:

- The FAGP mortar has a very good adhesion to the OPC substrate. Regardless of substrate condition, the failure mode of FAGP mortars from the slant shear test was either axial split or axial split-shear combined; the minimum shear bond strength for FAGP mortars was in the range of 3 MPa to 6 MPa, corresponding to a bond plane with a 45-degree inclination from vertical.
- The shear bond strength of FAGP is higher than that of OPC and commercially available geopolymer repair systems. Under dry substrate circumstances, the shear bond strength of FAGP reached 14 MPa, surpassing that of OPC and P-GP by 1.5 times.
- Rough surface profiles appeared to favour all mortar types between substrate conditions; however, P-GP mortar was unable to effectively penetrate the cavities of the roughened surface due to the diminished flow qualities of the fresh mortar.
- The OPC and P-GP bond characteristics were improved in the presence of moisture. Multiples in statistical analysis indicated that when overlaid on identical surface roughness conditions, the moisture level at the substrate (used in the current investigation) appeared to be irrelevant to the geopolymer-concrete shear bond strength. The synergistic effect of the Smooth-Saturated condition, on the other hand, appears to have a negative impact on the shear bond performance of the FAGP-based repair mortars.
- Despite being bonded on a smooth-saturated substrate, FAGP mortar-coated pipe segments demonstrated a consistent strain distribution (maximum of 0.6 %) across the surface area in the X and Y axes, up to 80 % of the ultimate load. Conversely, the surface strain began to differ at the bond line in both OPC and P-GP, resulting in the initiation of fractures at the bond line at an early stage, corresponding to 15–20 % of the ultimate load.
- The FAGP strain maps demonstrate no direct influence from acid exposure after 1000 hours on the repair coating. Although the visually seen damage to the OPC coating was obvious, the strain maps provided no clear evidence of the direct influence of acid exposure on the OPC repair bond. Despite this, a bond detachment was seen in the P-GP strain maps, appearing at the bond interface within the acid-exposed region, implying that acid permeation may have contributed to the debonding.

The current investigation of the adhesion characteristics of FA-based geopolymer mortars focused on the mechanical evaluation of the bond performance using a slant shear 35bond strength test. Future studies that investigate phase change and microscopy analysis at the bond interface will assist in understanding the bond performance under different substrate circumstances in detail. In bond durability experiments, exposure longer than 1000 hrs is recommended to simulate actual sewer conditions and generate a noticeable effect. Nevertheless, the results of this study demonstrated that FAGP mortar is suitable for sewer rehabilitation as it has very good adhesion to OPC substrate regardless of substrate condition.

CRedit authorship contribution statement

Allan Manalo: Writing – review & editing, Validation, Supervision, Conceptualization. **Piumika W. Ariyadasa:** Writing – original draft, Methodology, Investigation, Formal analysis, Data curation, Conceptualization. **Weena Lokuge:** Writing – review & editing, Supervision. **Vasantha Aravinthan:** Writing – review & editing, Supervision. **Kiru Pasupathy:** Writing – review & editing. **Andreas Gerdes:** Writing – review & editing, Supervision.

Declaration of Competing Interest

There is no conflict of interest in the submitted manuscript entitled “Bond performance of fly ash-based geopolymer mortar in simulated concrete sewer substrate”. All authors have approved the manuscript and agree with its submission to this journal. We guarantee that the contribution is an original material, has not been published previously and is not under consideration for publication elsewhere. All the materials and information contained in the paper are not restricted and are available to all.

Data availability

No data was used for the research described in the article.

Acknowledgement

Part of this research was supported by the SAGE Athena Swan Scholarship for Women in STEMM Research - University of Southern Queensland, Australia.

References

- [1] M. Lv, D. Gao, L. Yang, C. Li, J. Tang, Bond properties between concrete and high ductility cementitious composite with totally recycled fine aggregate, *Constr. Build. Mater.* 357 (2022) 129373.
- [2] M. Qasim, C.K. Lee, Y.X. Zhang, An experimental study on interfacial bond strength between hybrid engineered cementitious composite and concrete, *Constr. Build. Mater.* 356 (2022) 129299.
- [3] H. Abdulrahman, R. Muhamad, P. Visintin, A. Azim, Shukri, *Mechanical properties and bond stress-slip behaviour of fly ash geopolymer concrete*. *Constr. Build. Mater.* 327 (2022) 126909.
- [4] F. Pacheco-Torgal, Z. Abdollahnejad, S. Miraldo, S. Baklouti, Y. Ding, An overview on the potential of geopolymers for concrete infrastructure rehabilitation, *Constr. Build. Mater.* 36 (2012) 1053–1058.
- [5] M. Wu, T. Wang, K. Wu, L. Kan, Microbiologically induced corrosion of concrete in sewer structures: a review of the mechanisms and phenomena, *Constr. Build. Mater.* 239 (2020) 117813.
- [6] T. Wang, K. Wu, L. Kan, M. Wu, Current understanding on microbiologically induced corrosion of concrete in sewer structures: a review of the evaluation methods and mitigation measures, *Constr. Build. Mater.* 247 (2020) 118539.
- [7] T. Wells, R.E. Melchers, P. Bond, Factors involved in the long term corrosion of concrete sewers, in: *proceedings of the Forty Ninth Annual Conference of the Australasian Corrosion Association 2009: Corrosion and Prevention 2009* (2009).
- [8] R. Fearon, R. Cosgrove, *Infrastructure Cliff? Queensland's Ageing Water and Sewerage Assets. 2. cost implications for in-ground assets* (QWRAP Research Report 5.2), Local Government Association of Queensland: qldwater.com.au (2019) 2–34.
- [9] H. Zhu, T. Wang, Y. Wang, V.C. Li, Trenchless rehabilitation for concrete pipelines of water infrastructure: A review from the structural perspective, *Cem. Concr. Compos.* 123 (2021) 104193.
- [10] S. Feng, H. Xiao, J. Geng, Bond strength between concrete substrate and repair mortar: effect of fibre stiffness and substrate surface roughness, *Cem. Concr. Compos.* 114 (2020) 103746.
- [11] S. Feng, H. Xiao, H. Li, Comparative studies of the effect of ultrahigh-performance concrete and normal concrete as repair materials on interfacial bond properties and microstructure, *Eng. Struct.* 222 (2020) 111122.
- [12] M.S. Ali, A.K. Sachan, A review on the durability and applicability of Geopolymer concrete from the recent research studies, *Mater. Today.: Proc.*, 2022. 52 (2022) 911–922.
- [13] P. Cong, Y. Cheng, Advances in geopolymer materials: A comprehensive review, *J. Traffic Transp. Eng. (Engl. Ed.)* 8 (3) (2021) 283–314.
- [14] S. Samantasinghar, S.P. Singh, Strength and Durability of Granular Soil Stabilized with FA-GGBS Geopolymer, *J. Mater. Civ. Eng.* 33 (2021) 06021003.
- [15] G. Fahim Huseien, J. Mirza, M. Ismail, S.K. Ghoshal, A. Abdulameer Hussein, Geopolymer mortars as sustainable repair material: A comprehensive review, *Renew. Sustain. Energy Rev.* 80 (2017) 54–74.
- [16] T. Phoo-ngernkham, A. Maegawa, N. Mishima, S. Hatanaka, P. Chindaprasirt, Effects of sodium hydroxide and sodium silicate solutions on compressive and shear bond strengths of FA–GBFS geopolymer, *Constr. Build. Mater.* 91 (2015) 1–8.
- [17] H. Alanazi, M. Yang, D. Zhang, Z. Gao, Bond strength of PCC pavement repairs using metakaolin-based geopolymer mortar, *Cem. Concr. Compos.* 65 (2016) 75–82.
- [18] C. Phiangphimai, G. Joinok, T. Phoo-ngernkham, N. Damrongwiriyanupap, S. Hanjitsuwan, C. Suksiripattanapong, P. Sukontasukkul, P. Chindaprasirt, Durability properties of novel coating material produced by alkali-activated/cement powder, *Constr. Build. Mater.* 363 (2023) 129837.

- [19] F. Pacheco-Torgal, J. Castro-Gomes, S. Jalali, Adhesion characterization of tungsten mine waste geopolymeric binder. Influence of OPC concrete substrate surface treatment, *Constr. Build. Mater.* 22 (3) (2008) 154–161.
- [20] H. Abdulrahman, R. Muhamad, P. Visintin, A.A. Shukri, Mechanical properties and bond stress-slip behaviour of fly ash geopolymer concrete, *Constr. Build. Mater.* 327 (2022) 126909.
- [21] J. Tan, H. Dan, Z. Ma, Metakaolin based geopolymer mortar as concrete repairs: Bond strength and degradation when subjected to aggressive environments, *Ceram. Int.* 48 (16) (2022) 23559–23570.
- [22] M.H. Al-Majidi, A.P. Lampropoulos, A.B. Cundy, O.T. Tsioulou, S. Al-Rekabi, A novel corrosion resistant repair technique for existing reinforced concrete (RC) elements using polyvinyl alcohol fibre reinforced geopolymer concrete (PVAFRGC), *Constr. Build. Mater.* 164 (2018) 603–619.
- [23] H.Y. Zhang, V. Kodur, S.L. Qi, B. Wu, Characterizing the bond strength of geopolymers at ambient and elevated temperatures, *Cem. Concr. Compos.* 58 (2015) 40–49.
- [24] S. Samantasinghar, S.P. Singh, Fresh and Hardened Properties of Fly Ash–Slag Blended Geopolymer Paste and Mortar, *Int. J. Concr. Struct. Mater.* 13 (2019).
- [25] E. Gomaa, A. Gheni, M.A. ElGawady, Repair of ordinary Portland cement concrete using ambient-cured alkali-activated concrete: Interfacial behavior, *Cem. Concr. Res.* 129 (2020) 105968.
- [26] J.P. Gevaudan, B. Santa-Ana, W.V. Srubar, I.L.I. Iron, mineral admixtures improve the sulfuric acid resistance of low-calcium alkali-activated cements, *Cem. Concr. Compos.* 116 (2021) 103867.
- [27] W.G. Valencia-Saavedra, R. Mejía de Gutiérrez, F. Puertas, Performance of FA-based geopolymer concretes exposed to acetic and sulfuric acids, *Constr. Build. Mater.* 257 (2020) 119503.
- [28] P.L. Matthieu, A. Bertron, L. Auer, G. Hernandez Raquet, J.-N. Foussard, G. Escadeillas, A. Cockx, P. Etienne, An innovative approach to reproduce the biodeterioration of industrial cementitious products in a sewer environment. Part I: Test design, *Cem. Concr. Res.* 73 (2015) 246–256.
- [29] J. Tan, H. Dan, Z. Ma, Metakaolin based geopolymer mortar as concrete repairs: Bond strength and degradation when subjected to aggressive environments, *Ceram. Int.* (2022).
- [30] A. Ojha, P. Aggarwal, Durability performance of low calcium Flyash-Based geopolymer concrete, *Structures* (2023) (Elsevier).
- [31] D.P. Bentz, I. De la Varga, J.F. Muñoz, R.P. Spragg, B.A. Graybeal, D.S. Hussey, D. L. Jacobson, S.Z. Jones, J.M. LaManna, Influence of substrate moisture state and roughness on interface microstructure and bond strength: Slant shear vs. pull-off testing, *Cem. Concr. Compos.* 87 (2018) 63–72.
- [32] H. Beushausen, B. Höhlig, M. Talotti, The influence of substrate moisture preparation on bond strength of concrete overlays and the microstructure of the OTZ, *Cem. Concr. Res.* 92 (2017) 84–91.
- [33] C. Grengg, N. Ukrainczyk, G. Koraimann, B. Mueller, M. Dietzel, F. Mittermayr, Long-term in situ performance of geopolymer, calcium aluminate and Portland cement-based materials exposed to microbially induced acid corrosion, *Cem. Concr. Res.* 131 (2020) 106034.
- [34] H. Khan, M. Yasir, A. Castel, Performance of cementitious and alkali-activated mortars exposed to laboratory simulated microbially induced corrosion test, *Cem. Concr. Compos.* 128 (2022) 104445.
- [35] C. Zanotti, N. Randl, Are concrete-concrete bond tests comparable? *Cem. Concr. Compos.* 99 (2019) 80–88.
- [36] S. Austin, P. Robins, Y. Pan, Shear bond testing of concrete repairs, *Cem. Concr. Res.* 29 (7) (1999) 1067–1076.
- [37] L. Courard, T. Piotrowski, A. Garbacz, Near-to-surface properties affecting bond strength in concrete repair, *Cem. Concr. Compos.* 46 (2014) 73–80.
- [38] Purwanto, J.J. Ekaputri, Nuroji, B.R. Indriyantho, A. Han, B.S. Gan, Shear-bond behavior of self-compacting geopolymer concrete to conventional concrete, *Constr. Build. Mater.* 321 (2022) 126167.
- [39] A. AlHallaq, B. Tayeh, S. Shihada, Investigation of the bond strength between existing concrete substrate and UHPC as a repair material, *Int. J. Eng. Adv. Technol. IJEAT* 6 (2017) 210–217.
- [40] D. Daneshvar, A. Behnood, A. Robisson, Interfacial bond in concrete-to-concrete composites: a review, *Constr. Build. Mater.* 359 (2022) 129195.
- [41] W. Zailani, M. Abdullah, R. Razak, M. Zainol, M. Tahir. Bond strength mechanism of fly ash based geopolymer mortars: a review, in: *IOP Conference Series: Materials Science and Engineering*, 2017. IOP Publishing.
- [42] P. Ganesh, A.R. Murthy, Simulation of surface preparations to predict the bond behaviour between normal strength concrete and ultra-high performance concrete, *Constr. Build. Mater.* 250 (2020) 118871.
- [43] W. Lokuge, A. Wilson, C. Gunasekara, D.W. Law, S. Setunge, Design of fly ash geopolymer concrete mix proportions using Multivariate Adaptive Regression Spline model, *Constr. Build. Mater.* 166 (2018) 472–481.
- [44] C. Chen, W. Gong, W. Lutze, I.L. Pegg, Kinetics of fly ash geopolymerization, *J. Mater. Sci.* 46 (9) (2011) 3073–3083.
- [45] ASTM International, ASTM C 882/C 882M-05 Standard Test Method for Bond Strength of Epoxy-Resin Systems Used With Concrete By Slant Shear 2005, S&P Global. p. 4.
- [46] S. Wei, Z. Jiang, H. Liu, D. Zhou, M. Sanchez-Silva, Microbiologically induced deterioration of concrete: a review, *Braz. J. Microbiol.* 44 (4) (2013) 1001–1007.
- [47] ASTM International, ASTM C1437 Standard Test Method for Flow of Hydraulic Cement Mortar. 2015, S&P Global. p. 2.
- [48] ASTM International, ASTM C109 Standard Test Method for Compressive Strength of Hydraulic Cement Mortars (Using 2-in. or 50-mm cube specimens). 1983, S&P Global. p. 8.
- [49] ASTM International, ASTM F2551:2009:R2023 Standard practice for installing a protective cementitious liner system in sanitary sewer manholes, *Am. Soc. Test. Mater.* (2023) 4.
- [50] Standards Australia, AS/NZS 4058:2007 Precast Concrete Pipes (Pressure and non pressure). 2007, Standards Australia.
- [51] B. Liu, F. Yue, B. Chen, X. Man, L. Chen, S. Jaissee, Study on bond performance, flexural and crack extension behavior of base concrete prisms strengthen with strain-hardening cementitious composites (SHCC) using DIC technology, *Constr. Build. Mater.* 251 (2020) 119035.
- [52] R. Yang, Y. Li, D. Zeng, P. Guo, D.I.C. Deep, Deep learning-based digital image correlation for end-to-end displacement and strain measurement, *J. Mater. Process. Technol.* 302 (2022) 117474.
- [53] H. Zhu, K. Yu, V.C. Li, Sprayable engineered cementitious composites (ECC) using calcined clay limestone cement (L3C) and PP fiber, *Cem. Concr. Compos.* 115 (2021) 103868.
- [54] W.W. Ahmad Zailani, A. Bouaissi, M.M.A.B. Abdullah, R. Abd Razak, S. Yoriya, M. A.A. Mohd Salleh, M.R. Rozainy, M.A.Z., H. Fansuri, Bonding Strength Characteristics of FA-Based Geopolymer Paste as a Repair Material When Applied on OPC Substrate, *Appl. Sci.* 10 (9) (2020) 3321.
- [55] M.K. Al-Madani, M.A. Al-Osta, S. Ahmad, H.R. Khalid, M. Al-Huri, Interfacial bond behavior between ultra high performance concrete and normal concrete substrates, *Constr. Build. Mater.* 320 (2022) 126229.
- [56] W.W.A. Zailani, M.M.A.B. Abdullah, M.R.R.M.A. Zainol, R.A. Razak, M.F.M. Tahir, Compressive and bonding strength of fly ash based geopolymer mortar, *AIP Conf. Proc.* 1887 (1) (2017) 020058.
- [57] T. Phoo-ngernkham, V. Sata, S. Hanjitsuwan, C. Ridthirud, S. Hatanaka, P. Chindaprasit, High calcium fly ash geopolymer mortar containing Portland cement for use as repair material, *Constr. Build. Mater.* 98 (2015) 482–488.
- [58] A.M. Diab, M. Abd Elmoaty, M.R.T. Eldin, Slant shear bond strength between self compacting concrete and old concrete, *Constr. Build. Mater.* 130 (2017) 73–82.
- [59] Y. Shen, Y. Wang, Y. Yang, Q. Sun, T. Luo, H. Zhang, Influence of surface roughness and hydrophilicity on bonding strength of concrete-rock interface, *Constr. Build. Mater.* 213 (2019) 156–166.